# The Role of Alkylammonium Bromides on the Surface Passivation of Stable Alcohol-Dispersed $CsPbX_3$ Nanocrystals and on the Stability Enhancement in Light-Emitting Applications

*Pablo Uribe-Vegas,[1,#] Alexis Villanueva-Antolí,[2,#] Camilo Segura,[1,3] Francisca Werlinger,[1,4] Karen R. Aliaga,[4] Renato Caprile,[4] Oleksandra S. Trofymchuk,[4] Mario E. Flores,[1] Igor O. Osorio-Román,[1] Carlos Echeverría-Arrondo,[2] Samrat Das Adhikari,[2] Olfa Selmi[2], Iván Mora-Seró,[2] Jhonatan Rodriguez-Pereira,[5,6] Bapi Pradhan,[7] Michael Paulus[8], Christian Sternemann,[8] Johan Hofkens,[7] Javier Martinez,[1] Sofia Masi[2,*] and Andrés F. Gualdrón-Reyes[1,2,*]*

[1]Facultad de Ciencias, Instituto de Ciencias Químicas, Universidad Austral de Chile, Isla Teja, Valdivia, 5090000, Chile.
[2]Institute of Advanced Materials (INAM), Universitat Jaume I (UJI), Avenida de Vicent Sos Baynat, s/n, 12071 Castelló de la Plana, Castellón, Spain.
[3]Departamento de Química, Facultad de Ciencias, Universidad de Chile, Las Palmeras 3425, Ñuñoa, Región Metropolitana, Chile.
[4]Facultad de Ciencias Químicas y Farmacéuticas, Departamento de Química Orgánica y Fisicoquímica, Universidad de Chile, Santiago 8380492, Chile.
[5]Center of Materials and Nanotechnologies, Faculty of Chemical Technology, University of Pardubice, Nam. Cs. Legii 565, 53002 Pardubice, Czech Republic.
[6]Central European Institute of Technology, Brno University of Technology, Purkynova 123, Brno, 61200, Czech Republic.
[7]Department of Chemistry, KU Leuven, 3001 Heverlee, Belgium.
[8]Fakultät Physik/DELTA, Technische Universität Dortmund, 44221 Dortmund, Germany

**Abstract**

The ligand passivation is considered an attractive strategy to prepare high-quality perovskite nanocrystals (PNCs) with improved photophysical features in polar media. However, the long-term stabilization of PNCs in these environments is still challenging, being pivotal to understand the protection mechanism given by prominent surface ligands and to avoid the material deterioration in polar solvents. In this work, we investigated how the nature of diverse alkylammonium bromides used during surface passivation influences on the photophysical properties and quality of $CsPbX_3$ PNCs fully dispersed in alcohol environments, exhibiting stability up to 10 months. By adding didodecyldimethylammonium benzyldodecyldimethylammonium and tetrabutylammonium bromides (DDAB, BDAB and TBAB, respectively), we observe that DDAB and BDAB promote a suitable and partial surface coverage, respectively, suppressing defect sites in the nanocrystals. Conversely, TBAB shows a poor surface protection, decreasing the PL features of PNCs. The presence of DDAB and BDAB favors the fabrication of color converters, and efficient light emitting diodes (LEDs) with external quantum efficiencies (EQE) ~23%. Interestingly, a significant device stability with BDAB capping shows a LED half lifetime 20-fold

longer than for DDAB. This contribution offers a promising approach for preparing highly luminescent and stable alcohol-dispersed PNCs, useful to fabricate efficient optoelectronic devices.

## 1. Introduction

Perovskite nanocrystals (PNCs) have been recognized as the next generation of prominent colloidal semiconductors with mesmerizing defect-tolerant nature, modulable surface chemistry and improved optical/electronic features, in addition to their low-cost and facile synthesis procedures.[1] These characteristics have favored the preparation of nanoparticles (NPs) with high PL features and controllable band gap,[2, 3] guaranteeing the fabrication of light emitting diodes (LEDs) with external quantum efficiencies nearing to 30%,[4, 5] and perovskite quantum dots-based solar cells with efficiencies close to 20%.[6] Then, taking advantage of their UV-vis-NIR light absorption and carrier transport capabilities, PNCs are involved in photo(electro)chemical generation of $H_2$,[7, 8] $CO_2$ reduction for decarbonization processes,[9, 10] photocatalytic organic synthesis,[11, 12] and redox reactions to degrade toxic and recalcitrant organics.[13-15] In this context, PNCs are useful in a wide range of applications. However, they exhibit a notable limitation due to their ionic structure, which can deteriorate in the presence of oxygen, moisture, and polar environments.[16-18] In absence of a protective coverage, the direct interaction between the NPs and the polar medium damages the crystalline structure of the material, emerging a high density of structural defects, and quenching rapidly the intrinsic properties of the perovskite.[19, 20]

With the purpose of extending the stability of the perovskite in polar media, interesting approaches have been studied such as polymer matrix encapsulation,[21] to avoid the direct permeation of the polar molecules to reach the NPs surface. A stability record for PNCs systems has been reached by introducing methacrylate-based polymeric coverage for $MAPbBr_3$ PNCs, providing high resistance to organic, NaOH and HCl aqueous solutions for almost two years (600 days), keeping a PL quantum yield (PLQY) ~70%.[22] At this scenario, the low density of $H_2O$ molecules compensates halide deficiency in the NPs, being adequate to improve the PL properties. The addition of micellar surfactants is also a prominent option for PNCs stabilization, as the case of glycyrrhizic acid (GA).[23] Considering the restrained desorption capability of GA surfactant from PNCs surface, the perovskite composite is stable in MeOH ambient, with a PLQY ~85.3% and two-months stable in storage. Then, the addition of alternative ligands with higher binding capability to the NPs surface, as the case of the (3-aminopropyl)triethoxysilane (APTES), controls the perovskite particle size and induces a gradual steric hindrance in the surface to block the polar molecules mobility.[24] This effect can be easily reached by varying the APTES concentration, also avoiding the PNCs aggregation.[25] Meanwhile, novel synthetic routes based on ligand assisted reprecipitation process (LARP) have been highlighted to mediate the PNCs growth from ethanol (EtOH) solution, in the presence of Bis(2,4,4-trimethylpentyl)-phosphinic acid (TMPPA).[19] TMPPA can favor the emergence of polar Pb=O

or Pb–OH moieties, promoting the formation of inter-ligand hydrogen bonds with EtOH and $H_2O$ molecules. In this way, a barrier between the polar species and the PNCs core is produced, preserving the PL features of the PNCs. On the other hand, $CsPbBr_3$ clusters (CNC) have been also obtained by adding polyvinylpyrrolidone (PVP) in the LARP procedure, making the final product stable in alcohol solvents such as EtOH, isopropanol and organic acids for 30 days.[26] The appearance of Pb–O coordination in the presence of PVP is the key factor for ligand passivation of the NPs, improving their dispersibility in the polar solvents for photocatalytic degradation of dyes.

Interestingly, laser ablation in EtOH medium has been employed for the synthesis of ligand-free $CsPbBr_3$ PNCs, through two different approaches: first one denominated 2-step synthesis where $PbBr_2$ compressed powder is irradiated with a Nd:YAG laser at 355 nm, and then reacted with CsBr precursor dispersed in same alcohol.[27] Then, 1-step synthesis is based on a similar procedure to 2-step synthetic route, but CsBr is already present in the alcohol solvent before the ablation process. NPs can reach a maximum PLQY ~16%, with long-term stability for 15 days. Although these alternatives offer an ecofriendly and sustainable way to grow PNCs from the polar environment, the absence of alkylammonium species suppresses the radiative recombination, deteriorates the structure of the perovskite, and decreases the quality of the final material. Neither actual modified synthetic procedures nor the use of robust ligands cannot fully avoid the material deterioration in direct contact with polar medium.

Previously, we have explored the use of didodecyldimethylammonium bromide (DDAB) to stabilize PNCs in polar solvents.[28] We have observed that DDAB can protect the $CsPbX_3$ PNCs from a methanol/butanol (MeOH/BuOH) environment, reaching 100% PLQY and long-term stability up to 7 months (5040 h). DDAB mediates a ligand exchange with oleylammonium cations ($OLA^+$), which interacts with the alcohols to form alkoxide groups.[29-31] These species also contribute to the stabilization in polar solvents. Therefore, it is deductible that depending on the nature of the alkylammonium bromide (AlkylBr), different protection mechanisms would be achieved, impacting on the surface chemistry, PL properties, and stability of the PNCs in a polar medium. In this work we show the influence of AlkylBr nature on the PL and electronic properties $CsPbBr_3$ PNCs fully dispersed in a MeOH/BuOH system, achieving long-term stability up to 10 months under ambient conditions. By adding the PNCs into diverse concentrations of DDAB, benzyldodecylammonium bromide (BDAB) and tetrabutylammonium bromide (TBAB) (15, 85, and 200 mM) in BuOH, we infer that $DDA^+$ structure is suitable to provide a more efficient coverage than $BDA^+$ cation, where a partial passivation is promoted. Meanwhile, $TBA^+$ cation is prone to exhibit a high degree of steric hindrance, offering a poor surface coverage. Therefore, the direct interaction between the alcohols and NPs is mediated, quenching faster their PL features. Thus, DDAB and BDAB were studied for PNCs processability to fabricate polymeric color converters with PL stability ~4 h under a constant voltage, and active layers for green-LEDs with external quantum efficiencies (EQE) up to 23.2%. Interestingly the

operational LED half lifetime ($t_{50}$) depends strongly on the AlkylBr nature of surface passivating agent. This work makes it possible to comprehend the passivation mechanism given by the type of AlkylBr and provide a novel strategy for less-defective PNCs processing in polar solvents, being useful for the fabrication of more efficient and stable LED devices.

## 2. Results and discussion

With the aim to analyze the effect of the AlkylBr nature on the stabilization capability of $CsPbBr_3$ PNCs dispersed in alcohol environment along the time, we conducted transmission electron microscopy (TEM) and scanning electron microscopy (SEM) measurements. 500 µL of the colloidal PNCs dispersed in hexane (50 $mg \cdot mL^{-1}$) was added to a 2 mL of 85 mM DDAB, BDAB and TBAB ligands solutions in BuOH, and the resulting samples were studied under the following conditions: (i) MeOH (500 µL) + BuOH system at 0 h (as-prepared material) and (ii) MeOH (500 µL) + BuOH after 7300 h of aging. The molecular structure of each ligand is shown in **Scheme S1**. **Figure 1A–D** shows the typical TEM images of the as-prepared PNCs dispersed in the MeOH/BuOH medium (hereafter named as PNCs-$C_x$OH) in the absence and presence of the different AlkylBr ligands, where a nanocube shape is noted in all the samples. Nevertheless, the particle size and their corresponding distribution, see **Figure S1A–D**, is determined by the ligand nature. For pristine $CsPbBr_3$ PNCs, particle size is ~11.6 ± 2.7 nm, while DDAB-, BDAB- and TBAB-modified PNCs-$C_x$OH exhibited particle sizes ~6.8 ± 0.8 nm, 9.7 ± 1.0 nm, and 14.1 ± 3.2 nm, respectively. The detachment of oleic acid (OA) and oleylamine (OLA) from nanocrystals surface by the presence of the alcohol molecules generates aggregation to compensate the appearance of defect sites.[32] This is the reason to evidence big and non-uniform nanoparticles. On the contrary, the formation of smaller PNCs into the polar dispersion with high monodispersity in presence of DDAB is caused by partial exfoliation of surface $[PbBr_6]^{4-}$ octahedra units, restraining the perovskite growth.[33, 34] Low agglomeration is evidenced in this sample, corroborating the effective protection provided by this ligand in the alcohol medium.

On the contrary, bigger PNCs were obtained by introducing BDAB in the PNCs-$C_x$OH dispersion, suggesting a lower protection ability from this ligand to avoid the permeation of MeOH/BuOH molecules to reach the nanocrystals. Taking into account the existence of a benzyl group in $BDA^+$ cation unlike the linear dodecyl chain found in $DDA^+$, we suggest that the aromatic functionality mediates some steric hindrance in the PNCs surface to hinder the BDAB ligand passivation,[35] producing partial ligand-covered NPs and generating coalescence. However, a higher monodispersity and smaller particle size is estimated for this material (compared to pristine PNCs), indicating that BDAB can also restrain both the perovskite growth (exfoliation process) and the damage of its structural integrity. Conversely, in the case of adding TBAB, both higher average particle size and larger size distribution were obtained. We can deduce that poor ligand protection is established in the PNCs surface after the ligand exchange process, making more likely

the interaction between the alcohol molecules and the perovskite. This can also be noticed by the presence of spherical shapes in the TEM image of TBAB-PNCs-$C_x$OH dispersion, see **Figure 1D**, associated with the emergence of a different crystalline phase in the perovskite.[36] Through selected area electron diffraction (SAED) patterns, see **Figure S2A–D**, we corroborate the co-existence of the orthorhombic phase (ICSD 97851)[37] and 0D $Cs_4PbBr_6$ phase (ICSD 162158)[38] in the TBAB-PNCs-$C_x$OH dispersion, while the orthorhombic phase was only kept for the pristine, DDAB- and BDAB-PNCs-$C_x$OH. We conclude that both bulky DDAB and BDAB can prevent the fast alcohol diffusion to interact with the as-prepared PNCs than TBAB, where a closer contact with the polar molecules would be promoted.

**Figure 1A'–D'** shows the typical SEM images of the samples after 7300 h in the MeOH/BuOH medium, observing the formation of microcrystals. Interestingly, there are some differences between the microcrystal size and shape depending on the AlkylBr ligand nature. DDAB and BDAB produce smaller cubes than pristine one (0.5 ± 0.3 μm), with average sizes of 0.10 ± 0.09 μm and 0.10 ± 0.03 μm, respectively, see **Figure S1A'–C'**. Mainly, DDAB-PNCs-$C_x$OH sample depicts smaller particles after aging in alcohol, considering that a double purification was conducted in this work, making that more external ligands can cover the NPs (instant capping effect).[39] This fact suggests that both DDAB and BDAB ligands hinder the aggregation of PNCs exposed in the alcohol medium during the aging process, restraining the interaction with alcohol molecules. Meanwhile, rhombohedron-type microcrystals with a size of 0.4 ± 0.4 μm and high polydispersity are formed in the presence of TBAB, as a result of the fast particle agglomeration, **see Figure S1D'**. As discussed above, TBAB cannot provide effective ligand coverage in the PNCs, which can favor the coalescence of the NPs. Although some of the AlkylBr ligands can protect the $CsPbBr_3$ NPs from the polar environment, some of the alcohol molecules diffuse progressively through the organic coverage, generating the emergence of bigger particles.

Synchrotron-assisted grazing incidence wide angle X-rays scattering (GIWAXS) was used in as-prepared PNCs films dried at ambient air, to resolve in depth the crystalline structure of the samples, **Figure 1E** and **Figure S3A–D** depict the azimuthally integrated GIWAXS data (q) ($q_{xy}$) and the 2D circular integrated 1D patterns (($q_{zr}$ ) versus $q_z$) of films in the absence and presence of AlkylBr ligands, detailing the typical diffraction patterns at 1.07, 1.51, 2.15, 2.40, 2.62, 3.03, 3.21 and 3.72 $Å^{-1}$ corresponding to the [020; 101], [121; 200; 002], [040; 202], [141; 301; 222; 103], [240; 042; 321; 123], [242; 004], [341; 420; 143], [161; 402; 323; 204] and [044; 440] planes of the orthorhombic phase. No traces of 0D perovskite are detected. However, low-intense peaks were also found at smaller q values with certain periodicity in 1D pattern for BDAB- and TBAB-PNCs, accompanied by the appearance of new signals into 2D GIWAXS pattern at low q. This fact is commonly attributed to the formation of 2D perovskites[40] during surface exfoliation in the presence of BDAB and TBAB ligands. Therefore, we can establish that the presence of alcohol molecules can delay the octahedra exfoliation, preserving the 3D structure of the perovskite.

The optical features of the $CsPbBr_3$ PNCs were also influenced by the type of AlkylBr species used for the material stabilization. For this aim, we studied three diverse ligand concentrations in the MeOH/BuOH system: 17, 85, and 200 mM. As seen in **Figure 1F–H**, the absence of ligands generates a PL peak position at ~529 nm, with a low emission intensity. This behavior is typical of aggregated particles, a product of ligand removal from their surface, which generates an eventual PL quenching.[41] A PL quantum yield (PLQY) of 48% was achieved. However, the incorporation of DDAB and BDAB induces a slight blueshift in the PL of PNCs-$C_x$OH dispersions (at 523 and 521 nm, respectively), accompanied by a higher/slight decrease in the emission intensity, respectively at higher ligand concentrations, and the appearance of an emission shoulder at ~535 nm. First, the displacement of PL emission to smaller wavelengths is attributed to a strong quantum confinement regime achieved by the $[PbBr_6]^{4-}$ exfoliation in the perovskite surface, which agrees with the blueshift of the absorption edge noted in the UV-vis spectra of samples with DDAB and BDAB ligands,[42] see **Figure S4**. Simultaneously, the above ligands can suppress surface defect sites in the PNCs (mainly halide vacancies), increasing the PL of the photomaterial. Therefore, a PLQY of 100% was reached in both cases.

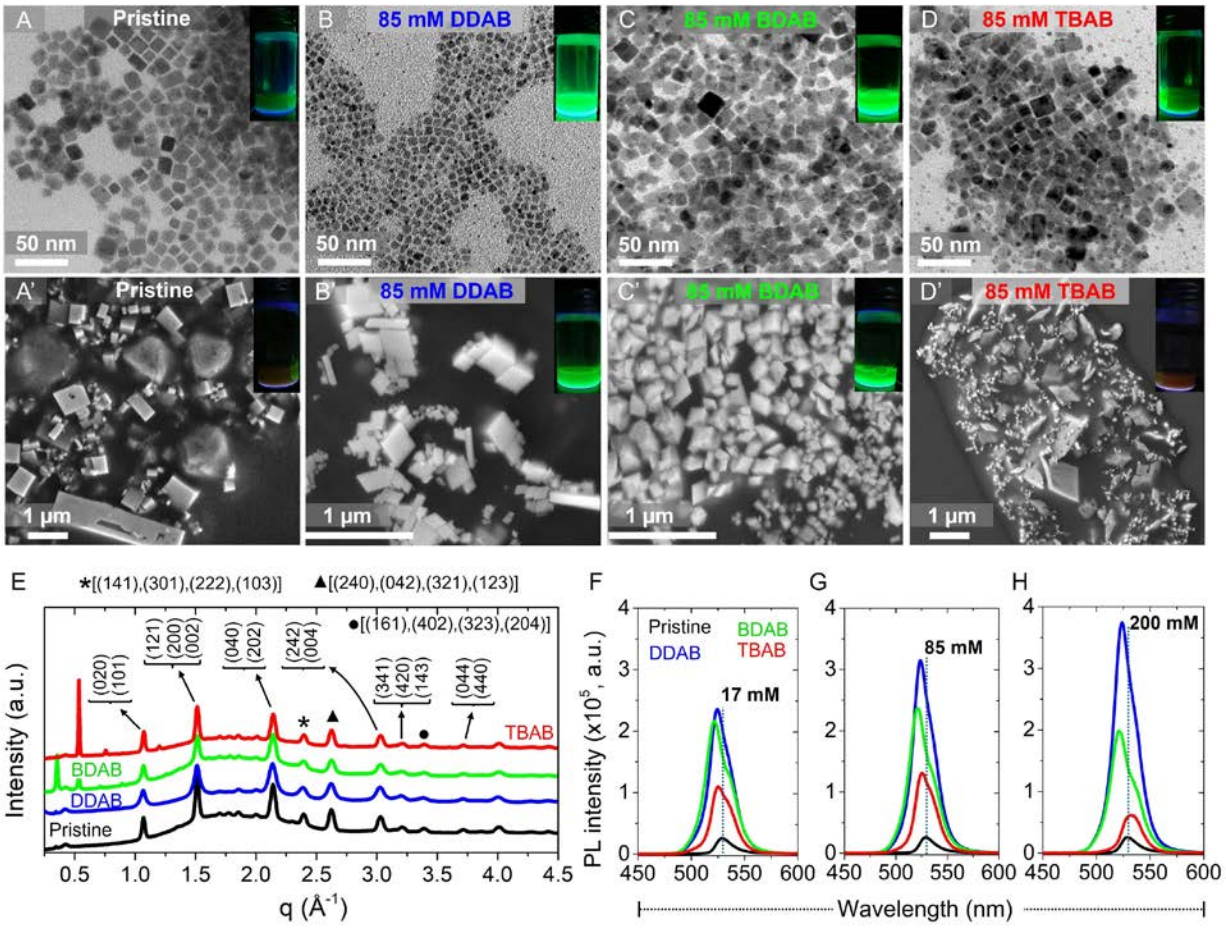

**Figure 1.** Typical (A-D) TEM images of $CsPbBr_3$ PNCs dispersed in MeOH/BuOH polar environment at 0 h, and corresponding (A'–D') SEM images of the samples after 7300 h aging in the alcohol medium, in (A,A') absence and presence of the AlkylBr ligands: (B,B') DDAB, (C,C') BDAB and (D,D') TBAB. The inset of Figures (A–D) and (A'–D') shows the luminescence of as-prepared and aged nanocrystals, respectively. (E) 1D line cuts from azimuthally integrated 2D GIWAXS patterns of $CsPbBr_3$ PNCs in the polar environment in the presence and absence of AlkylBr ligands. PL spectra of PNCs dispersions by varying the concentration of the AlkylBr ligands: (F) 17 mM, (G) 85 mM and (H) 200 mM.

However, the low degree of aggregation, homogeneous particle size and small size distribution with DDAB as seen through TEM images, see **Figure 1** and **Figure S1**, indicate a better surface protection and thereby, a lower intensity of the emission shoulder, unlike to the presence of BDAB, where a bigger particle size and larger size distribution were obtained. The partial surface passivation can induce some particle agglomeration, being more prominent this PL signal, but this coverage is enough to avoid the PNCs-alcohol contact, as we have confirmed through PLQY. On the other hand, TBAB mediates a slight blueshift in the PL emission at 17 and 85 mM while a redshift was achieved in the PL at 200 mM respect to DDAB and BDAB (also seen in the UV-vis spectrum with the emergence of scattering, see Figure S4), with lower emission intensity than pristine one. At this point, the PL shoulder found in DDAB and BDAB cases, now is the characteristic PL of PNCs in presence of TBAB at the highest concentration, indicating the highest degree of aggregation and the poorest effectiveness to enhance the radiative recombination. Thus, a PLQY of 58% was obtained, widely lower than those of its DDAB and BDAB analogous. Then, in terms of PL intensity of the PNCs-CxOH dispersions, DDAB and BDAB favor the increase and slight diminution of this optical feature, respectively, corroborating an efficient surface passivation in the polar solvent. Meanwhile, the lowered PL in PNCs with TBAB is ascribed to its possible strong steric hindrance produced on the PNCs surface, facilitating the diffusion of a high density of MeOH/BuOH molecules reaching perovskite core.

Then, the stability of $CsPbBr_3$ PNCs was studied through their PL features along the aging time, in function of the AlkylBr ligand added to the PNCs-$C_x$OH dispersions, see **Figure S5 and Figure S6.** For this aim, PL measurements were initially performed on the PNCs dispersed in BuOH at 0 and 1 h in the absence of MeOH. Later, controlled volumes of MeOH were added to the corresponding dispersions at 3 and 7 h, (200 and 300 µL MeOH, respectively), completing a total volume of 500 µL. Lastly, the prepared PNCs-$C_x$OH dispersions were aged for a longer time to achieve a maximum time of 7300 h, At this point, the influence of the AlkylBr concentration on the green emission of the $CsPbBr_3$ PNCs was analyzed through changes in the relative PL intensity as seen in **Figure S7**. In absence of AlkylBr ligands, the emission intensity of the NPs is redshifted and progressively quenched, see **Figure S5.** We attribute this behavior to the gradual detachment of OA/OLA ligands, facilitating the diffusion of the alcohol molecules,

and compromising the integrity of the NPs.[43] This direct interaction would mediate the appearance of diverse particle sizes, agreeing with the wide particle size distribution seen by TEM.

Later, the addition of AlkylBr capping agents in the PNCs-$C_x$OH dispersions hinders the fast deterioration of the PL properties of the NPs. As seen in **Figure S6A–C and Figure S7A**, the presence of DDAB avoids the decrease of the PL of the PNCs during the first couple of hours, and later the emission intensity is increased. As expected, the higher the DDAB concentrations, the better the PL intensity, indicating that the nonradiative recombination is supressed by removing A-site cation and X-site anion.[28] In the case of BDAB, a similar behavior was found during the first 7 h of analysis, also observing the increase of emission intensity for a longer aging time, see **Figure S6A'–C', Figure S7B**. However, this optical property was lower than DDAB by comparing the lowest concentration (17 mM) and eventually, the PL emission was slightly decreased at higher BDAB contents (85 and 200 mM). Accordingly, we suggest a partial coverage provided by BDAB, deducing that low concentrations of this ligand could favor the surface passivation. Although the steric hindrance given by benzyl groups restrains the fact to introduce a high density of BDAB molecules, these functional moieties also would offer a protection of nanocrystals against the harsh environment. This is in good agreement with the small particle size of BDAB-capped PNCs-$C_x$OH after 7300 h, avoiding material agglomeration as result of the protective effect of BDAB. Lastly, although the main PL emission (and therefore the relative PL intensity) of PNCs-$C_x$OH is quenched during the first couples of hours (0–24 h), independently of the TBAB concentration, a new signal at ~460 nm emerges, making that the PL emission of $CsPbBr_3$ slightly increases at longer aging times (24–7300 h), see **Figure S6A''–C'', Figure S7C.** This effect is more visible at the lowest ligand concentration (17 mM, see Figure S6A''). The new emission peak is attributed to the formation of 0D $Cs_4PbBr_6$ perovskite,[44] which has been reported to act as a protective layer to suppress the nonradiative recombination in $CsPbBr_3$.[45] Nevertheless, by raising up the TBAB concentration to 85 or 200 mM (Figure S6B'', C''), the appearance of 0D perovskite signal is hindered, inferring a better surface passivation (adequate ligand content to obtain the highest initial PL intensity), or the damage of the structural integrity of PNCs by a stronger steric hindrance of TBAB (excess of ligands), respectively. Despite to observe the abovementioned scenarios in function of TBAB concentration along the aging time, the surface protection provided by this ligand is not effective compared to DDAB and BDAB. At this point, we conclude that both DDAB and BDAB are prominent surface ligands to extend the stability of $CsPbBr_3$ PNCs for around 10 months, being this value longer than the previous report addressed for the alcohol-stabilized $CsPbX_3$ PNCs in absence of any encapsulation.[28]

To study the effect of the AlkylBr ligands on the chemical environment and composition of the $CsPbBr_3$ PNCs-$C_x$OH dispersions, X-ray photoelectron spectroscopy (XPS) analysis was performed. The concentration of all the ligands was fixed at 85 mM for comparative purposes. In all the samples, it was

identified the co-existence of C, O, N, Cs, Pb, and Br elements, see the corresponding XPS survey spectra in **Figure S8**. Then, the composition of the NPs dispersions is summarized in **Table S1**. **Figure 2A** depicts the high-resolution (HR) XPS Cs 3d spectra of the PNCs-$C_xOH$ dispersions in absence and presence of DDAB, BDAB and TBAB, observing a doublet at 724/738 eV. This signal is ascribed to Cs $3d_{5/2}$ and Cs $3d_{3/2}$ core levels, indicating the presence of $Cs^+$ cations contained into the $CsPbBr_3$ nanocrystals.[46] Meanwhile, **Figure 2B** shows the HR-XPS Br 3d spectra of the PNCs samples, where a doublet at 68/69 eV was associated with the Br $3d_{5/2}$ and Br $3d_{3/2}$ core levels. These signals indicate the formation of Pb-Br bonds coming from $[PbBr_6]^{4-}$ octahedra in the PNCs.[47] On the other hand, the HR-XPS N 1s spectra of pristine, DDAB, BDAB and TBAB-capped PNCs show a signal located ~401 and 402 eV, associated with amine moiety and the alkylammonium species corresponding to each ligand,[48] see **Figure 2C**. This allows us to infer that AlkylBr ligands promotes the generation of free OLA, exhibiting a higher content for TBAB. Later, attending to **Table S1**, a Cs, Br and N deficiency is noted in the pristine PNCs, corroborating the deterioration of the surface stoichiometry of the NPs in the polar solvent. However, the presence of the AlkylBr ligands increases the fraction of Br and N, deducing a better ligand coverage in the PNCs surface to compensate for the $Cs^+$ and halide vacancies. This fact corroborates the passivation effect of the capping agents to protect the integrity of the PNCs against MeOH/BuOH environment.

**Figure 2D** depicts the HR-XPS Pb 4f spectra of pristine and AlkylBr-capped PNCs-$C_xOH$ dispersions, observing the Pb $4f_{7/2}$ and Pb $4f_{5/2}$ core levels at 138/143 eV, respectively. These signals are attributed to the existence of $Pb^{2+}$ coming from the $[PbBr_6]^{4-}$ octahedra composing the perovskite structure. No undercoordinated Pb is seen in all the samples including the pristine one, indicating that the X-site positions into the octahedra building blocks are fully compensated either by adding carboxylate species from methyl acetate during washing process or/and ligand passivation from AlkylBr.[28] On the other hand, the total oxygen-to-bromine and total oxygen-to-lead ratios [denoted as $O_{total}/(Br+O_{total})$ and $O_{total}/(Pb+O_{total})$, respectively] are higher in the following order: DDAB < BDAB < TBAB, see **Figure 2E**. This behavior indicates that DDAB blocks the diffusion of a high density of MeOH/BuOH molecules to reach the NPs more efficiently, decreasing the oxygen content in the perovskite surface. Later, a lower N content is found in the presence of BDAB, reinforcing the hypothesis that the steric hindrance given by benzyl groups avoids the attachment of $BDA^+$ cations. On the contrary, a higher N content in the samples is obtained in the presence of TBAB, an indication of a high density of $TBA^+$ species surrounding the material surface. Although both the BDAB- and TBAB-capped PNCs-$C_xOH$ samples exhibit a close $O_{total}/(Br+O_{total})$ and $O_{total}/(Pb+O_{total})$ ratios, BDAB preserves the PL properties and extends the stability of the PNCs, while the optical properties of the perovskite are quickly quenched with TBAB ligand. Simultaneously, the above fractions for BDAB are higher than pristine sample, indicating the possibility of higher density of $R\text{-}O^-$ species on the perovskite surface. In this context, while BDAB can stabilize the structure of the PNCs even

though some alcohol molecules permeate through the ligand coverage, TBAB offers a poorer protection, making that NPs experience a change of crystalline phase, taking into account the release of free OLA. We believe that both the change of the surface stoichiometry by introducing TBAB and the direct interaction with a higher density of alcohol molecules are the reason to facilitate the formation of $Cs_4PbBr_6$ perovskite. The formation of a secondary crystalline structure during the surface passivation given by a particular type of AlkylBr ligand in polar media, will be focused on future works related to this research topic. Accordingly, we conclude that the addition of DDAB and BDAB is crucial to maintain the structural integrity and intrinsic properties of the PNCs in the alcohol environment, where a different passivation mechanism is carried out by these capping agents.

We have already reported that DDAB mediates a partial ligand exchange with native $OA^-$ and $OLA^+$ ligands covering initially the PNCs surface, generating free OA and OLA through the acid-base reaction equilibrium.[28] Later, after the addition of MeOH to the perovskite dispersion, OLA is able to ionize a fraction of the alcohol species forming the corresponding alkoxide ($R\text{-}O^-$) anions, which together with $Br^-$ species from the alkylammonium capping agents, stabilize the final product by filling halide vacancies.[28] To understand the protection mechanism given by the AlkylBr ligands in the MeOH/BuOH system, Nuclear Magnetic Resonance (NMR) spectroscopy measurements were performed. To distinguish the corresponding NMR resonances, the analysis was carried out on AlkylBr ligands (85 mM) with and without the presence of the $CsPbBr_3$ PNCs for comparative purposes. In this way, the corresponding description of NMR resonances of the OLA/OA system in absence and presence of PNCs, see **Figure S9A**, is discussed in supporting information.

Attending the typical NMR resonances of the individual DDAB ligand seen at $\delta$ = 3.53 and 3.43 ppm, see **Figure 2F**, associated with the methylene and methyl groups linked to quaternary N from the $-NR_3^+$ moiety,[49] these signals were considerably shifted to lower chemical displacement in the presence of the polar solvent (BuOH) and/or PNCs. Simultaneously, the NMR resonance of $OLA^+$ cations is absent, and a signal at $\delta$ = 1.90 ppm is attributed to free OA, see **Figure 2F.** These results, together with the changes in the signals from DDAB, are evidence of the ligand exchange between the AlkylBr ligand and $OLA^+/OA^-$ species in the NPs surface, replaced by $DDA^+/Br^-$ ions, respectively. By adding deuterated methanol (MeOD) in the DDAB-capped PNCs dispersed in BuOH to reach progressively a total volume of 35 µL, it is noticeable that the methyl and methylene resonances of DDAB and free OA are unprotected, being still absent the resonance of $OLA^+$. After adding 140 µL, a low-intense signal at 3.22 ppm appears, ascribed to free OLA**.** From these results, we can establish that a high density of $OLA^+$ produced by the interaction between OLA (obtained after ligand exchange) and alcohol species is linked to the defective PNCs surface, providing an efficient ligand coverage. This is one of the pivotal explanations for the material stabilization in alcohol environments.

To analyze the NMR spectra of BDAB-capped PNCs samples, we first identified the typical resonances of methylene (from the hydrocarbon chain) and methyl protons from individual BDAB, appearing at δ = 3.55 and 3.33 ppm, respectively, see **Figure 2G**. Compared to DDAB, additional signals are detailed at δ = 7.68–7.49 and 5.11 ppm, ascribed to protons from the aromatic ring and methylene from benzyl group, close to the ammonium moiety, respectively. In the presence of the polar solvent and perovskite, all BDAB resonances exhibit a shift in the chemical displacement to lower values, indicating the direct interaction between the ligand and the material surface. It is worth noting the existence of $OLA^+$ in the sample, since the emergence of a shoulder at δ = 3.06 ppm, accompanied by the resonance of the olefinic region of $OA^-$ and free OA species, at δ = 2.09 and 1.98 ppm, respectively. As expected, the $OLA^+$ resonance becomes more visible and shielded by dosing the NPs dispersion with MeOD, indicating that more $OLA^+$ is produced after alcohol ionization, see **Figure 2G**. However, after adding a higher MeOD volume up to 15 µL, the -$CH_2$ resonances from hydrocarbon chain and benzyl group are more resolved and shifted to lower chemical displacements, disappearing the $OLA^+$ signal. Here, we infer the presence of free BDAB species. Furthermore, as seen in **Figure S9B**, the NMR signal associated with alcohol species (in this case BuOH) in the presence of BDAB is highly shielded compared to other AlkylBr ligands (δ = 3.14 ppm), suggesting a stronger interaction between BDAB and the alcohol molecule.

In light of the present results and considering the existence of free BDAB (mediated by steric hindrance of benzyl groups on the material surface), we propose that a fraction of $BDA^+$ can interact with exchanged $OA^-$ ions released after ligand exchange to form $BDA^+OA^-$ species. In this context, the lower the density of free $OA^-$, the lower the density of released $OLA^+$ to form available OLA, hindering the subsequent alcohol ionization. At this point, it is also feasible the interaction between $BDA^+$ and some $R\text{-}O^-$ species, being able to replace $OLA^+$ and $OA^-$ linked to the NPs. This behavior can explain the cyclic behavior of $OLA^+$ and $OA^-$ resonances (emergence/absence) by adding more MeOD (20–140 µL). In this cyclic process, some alcohol molecules can also mediate the ligand detachment, causing some deterioration of the perovskite.

Lastly, in the case of TBAB, see **Figure S9C**, a typical triplet is observed for the individual ligand at δ = 3.41 ppm, attributed to the methylene directly linked to the nitrogen atom into the $-NR_3^+$ group, being this resonance shifted to lower values after the incorporation of the PNCs/BuOH. Then, by dosing the samples with MeOD, a broader and shielded NMR signal at δ = 3.09–3.03 ppm is observed, associated with released $OLA^+$ cations, Moreover, the $OA^-$ resonance is also detailed in all the NMR spectra by increasing the MeOD volume. We deduce that the alcohol molecule mediates the detachment of $OLA^+/OA^-$ from the material surface, even in the presence of the ligand, which agrees with high density of free OLA found by XPS, **Table S1**. According to the fast lowering of the PL features in TBAB-capped PNCs-$C_xOH$ dispersions, the coverage offered by this ligand is not enough to avoid the percolation of polar molecules to reach the

material, inducing a poor surface passivation. Thus, the formation of alkoxide species through free $OLA^+$ is a pivotal passivation mechanism to stabilize the PNCs dispersions in alcohol environments.

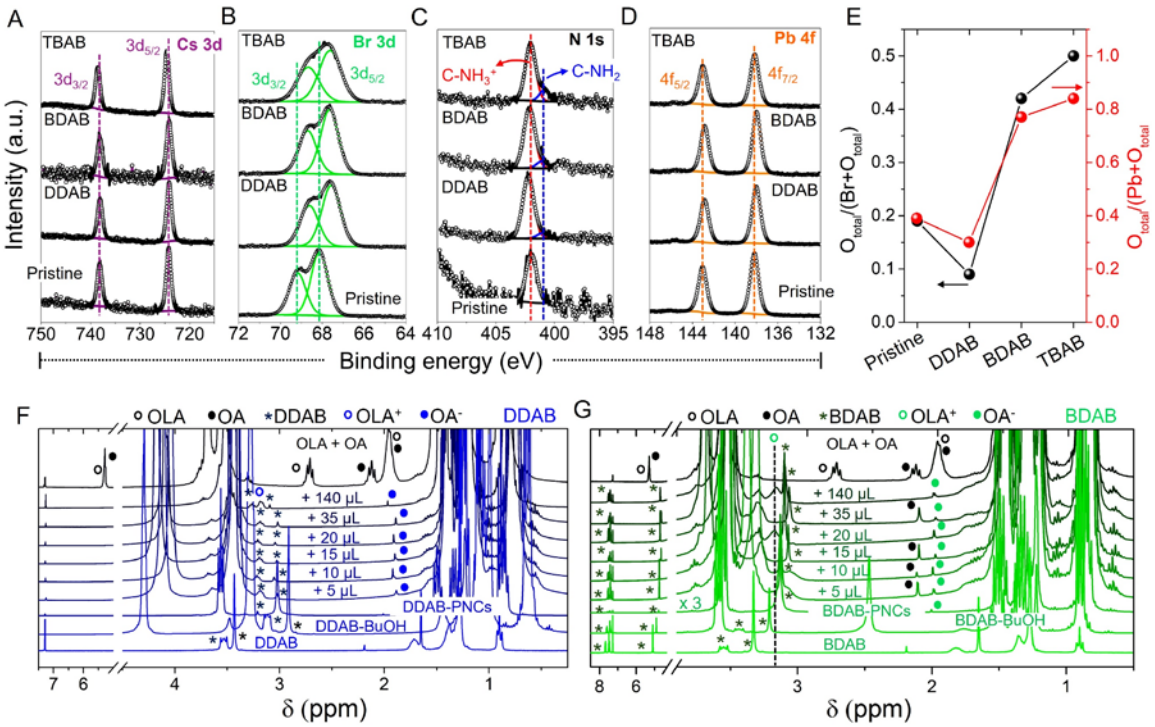


**Figure 2**. High-resolution XPS (A) Cs 3d, (B) Br 3d, (C) N 1s, (D) Pb 4f and (E) estimated total oxygen-to-halide/total oxygen-to-total lead ratios, for the $CsPbBr_3$ PNCs in the presence and absence of the AlkylBr ligands. $^1H$ (300 MHz, $CDCl_3$, 298 K) NMR spectra of $CsPbBr_3$ PNCs in absence and presence of (F) DDAB (blue spectra) and (G) BDAB (green spectra), dispersed in protic BuOH and titrated with different volume (µL) of deuterated methanol (MeOD). The concentration of ligands into BuOH solvent was 85 mM. The corresponding NMR spectra of (OA+OLA)/BuOH and AlkylBr/BuOH samples without perovskite were obtained for comparative purposes.

To validate the capability of the different AlkylBr capping to trigger the ligand exchange on PNCs surface, density functional theory (DFT) calculations were performed. Details for the DFT setup are described in supporting information. Based on the experience of determining the feasibility of replacing surface $OLA^+/OA^-$ species by presence of DDAB,[28] we also analyze the introduction of BDAB and TBAB, both in the presence of MeOH molecules. First, we prepared the initial system in the absence of any AlkylBr ligands, which consisted of a $CsPbBr_3$ slab with two $Cs^+$ defects and four $Br^-$ vacancies. While the $Cs^+$ deficiency is compensated with $OLA^+$ species, two $Br^-$ defects are filled with $OA^-$ ions, leaving two free $Br^-$ vacancies, see **Figure S10A**. By introducing the AlkylBr and MeOH species, two alkylammonium cations

from the corresponding ligands can exchange with the two $OLA^+$ sites, while $MeO^-$ anions replace the two $OA^-$ positions. Subsequently, $Br^-$ coming from the ligands compensate the remaining two Br vacancies. In this process, free OA is generated, while $OLA^+$ cations are linked to surface $Br^-$ species, see **Figure S10B–D**.

Then, we calculated the energy difference (ΔE) between initial and AlkylBr-modified systems ($E_I$ and $E_{LM}$, respectively) taking values of –0.86 eV and 1.16 eV in the presence of BDAB and TBAB, respectively. Surprisingly, the more negative ΔE provided in BDAB-capped PNCs *vs.* DDAB one (–0.49 eV, previously reported[28]) implies that the surface passivation is thermodynamically more favorable by the addition of BDAB. This fact would be likely since the $BDA^+$ cation (according to Lewis theory) is a stronger acid than $DDA^+$ due to aromatic ring containing the benzyl group offers a negative inductive effect on the adjacent methylene close to nitrogen. Therefore, the electron donation ability towards nitrogen decreases, increasing the acidity of the $-NR_3^+$ moiety and thereby, making its binding to perovskite stronger. However, the fact that the PL properties are more prone to quench in the alcohol medium, and the N content is the lowest found in the material surface, see **Table S1**, allows us to consider that a low density of this ligand is not linked to the perovskite surface, due a small degree of space occupied by the benzyl group. In the case of TBAB, the entire ligand structure is prone to cover a considerable part of the perovskite surface, generating a higher degree of steric hindrance. This could explain the highest content of amine moiety found by XPS, as result of free OLA, indication of the detachment of a high density of $OLA^+/OA^-$ from PNCs surface. At this point, it is expected to achieve a poor surface protection given by TBAB, favoring the degradation of the PNCs in the polar solvent. Hence, we conclude that DDAB and BDAB are suitable AlkylBr ligands to protect the NPs surface, stabilizing their PL features against the interaction with alcohol molecules.

For a further insight about how the AlkylBr ligands influence on the carrier recombination kinetics of PNCs-$C_x$OH samples, time-resolved PL measurements were performed. As seen in **Figure S11**, bi-exponential PL decays were measured in all cases. We believe, however, that the longer component is not the characteristic of the different carrier recombination rate but appears because of the PL decay lengthening due to an optical effect, more exactly, light scattering resulting in longer PL light pass inside the solution and therefore more efficient re-absorption/re-emission effect retarding the PL intensity decay.[50] In such a case, we characterize the PL decay kinetics only by the faster decay components, which are 8.80, 12.9, 13.6 and 8.05 ns for pristine, DDAB, BDAB and TBAB samples, respectively. Note that the highest PLQY values correspond to the longer lifetimes, and approximately two-fold lifetime shortening for pristine and TBAB samples correlates with the corresponding PLQY decrease. A longer lifetime with a 100% PLQY obtained for DDAB and BDAB corroborates the suppression of nonradiative channels by action of these ligands, indicating an efficient surface passivation by the introduction of $Br^-$ and $R\text{-}O^-$ species to fill halide defect sites.[30, 51]

After detailing the final photophysical features of the DDAB- and BDAB-capped PNCs-$C_xOH$ dispersions, we investigated these materials for light emitting applications: i) down-converting systems and ii) LEDs. For the first kind of system for on-chip application, we have embedded the corresponding PNCs dispersions into a commercial acrylate-based polymeric resin, perovskite:resin volume ratio = 4:1, and deposited the blend on a blue emitting LED chip, 3 W and wavelength: 445−450 nm, see supporting information for further details. Under the operation of the LED chips, part of the blue-emission is transmitted, while the rest of the light is absorbed by the AlkylBr-modified PNCs, converting it into green emission. Then, we proceed to analyze the stability of green-LED chips by varying (i) the applied voltage to modulate the PL emission intensity and later (ii) the change of the operation time to study the retention of the initial luminescence.

As seen in **Figure 3A,A'**, the PL of the color-converting DDAB- and BDAB-PNCs layer, with a PL peak position at 521 nm in both cases, is increased as the blue-light intensity from the LED chip raise up by applying a voltage up to 3.5 V. Later, a lower decrease in PL was achieved at higher energy (4.0 V). This behavior is typical for an efficient blue-to-green light conversion from the modified PNCs.[52] At this point, a better light conversion is achieved for the DDAB-LED system, indicating a favored radiative recombination into the perovskite layer. However, by analyzing the stability of the PL emission of the AlkylBr-LEDs under continuous irradiation at 3.0 V in the blue-LED chip for 4 h, we evidenced a longer PL stability in the BDAB-LED compared to DDAB-LED, see **Figure 3B,B'** and **Figure S12A**. **Inset of Figure 3B,B'** shows the respective green-LEDs under operation. The detachment of some ligands from the surface at prolonged irradiation flux is the common reason to mediate the decrease of the PL from the active layer.[53] This is reasonable for $DDA^+$ since this capping shows a lower binding ability to PNCs surface than $BDA^+$, as we have established from DFT calculations.

Taking advantage of the improved intrinsic properties of the AlkylBr-capped PNCs-$C_xOH$ dispersions, we were interested in preparing mixed halide $CsPbBr_{3-x}I_x$ PNCs inks by combining these PNCs samples with a fixed volume of $CsPbI_3$ colloidal solution. In this context, we studied the optical features of sensitive iodide-based PNCs layers for down-converting luminescent optoelectronics. As seen in **Figure 3C,C'**, the addition of 500 µL $CsPbI_3$ PNCs caused a redshift of the PL emission in both kinds of color-converting materials, but the degree of displacement was contrasting each other. In the case of DDAB-LEDs, a broad PL signal located at ~588 nm was reached, covering the green-yellow-red region of the energy spectrum. Accordingly, white-light emission was noted in the device, see **Inset of Figure 3C**. Conversely, the BDAB-LED produces a narrower PL at longer wavelengths, with emission peak position ~632 nm. Here, a reddish light emission was detected from the LED chip, see **Inset of Figure 3C'**. This discrepancy can be explained in terms of the ability of the AlkylBr to facilitate the anion-exchange (A-E) process between iodide and bromide species in the NPs surface. As we highlighted in **Figure S13**, we have explored the combination

of each DDAB- and BDAD-capped $CsPbBr_3$ PNCs dispersed in BuOH, with an iodide source as the case of potassium iodide (KI) dissolved in MeOH. By dosing the AlkylBr-PNCs with the iodide compounds, the PL of the initial materials was redshifted, depicting a more appreciable change in the presence of BDAB, even with a lower iodide dosage. We can deduce that DDAB provides a better compensation for Br deficiency, giving more content of this halide for the exchange dynamics, compared to BDAB, which can partially suppress the $Br^-$ defects. Therefore, there would be more available halide vacancies to fill with external iodide (KI or $CsPbI_3$). Nevertheless, the stability of the A-E-AlkylBr-PNCs displays more beneficial effect in the presence of BDAB, retaining the initial PL of the device for a longer time, see **Figure S12B.** At this stage, the stronger ability of $BDA^+$ cation to the PNCs surface confers a better resistance to the color converter, enhancing the operational stability of the LED.

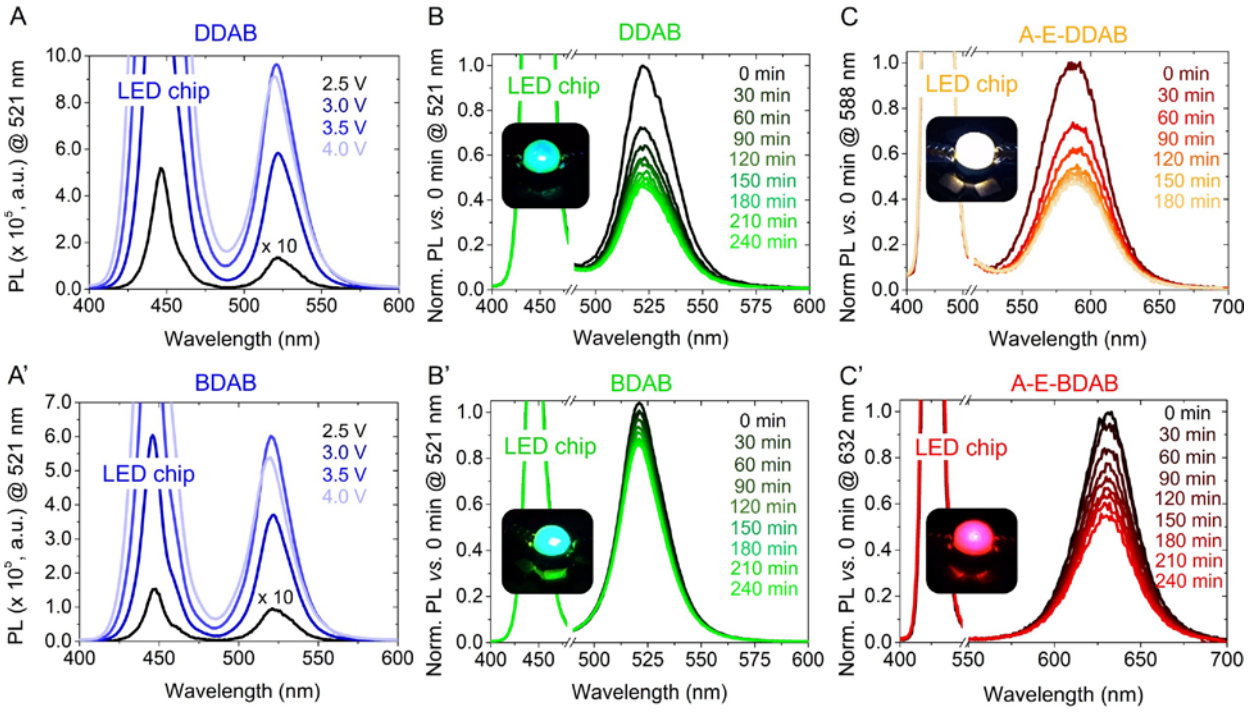


**Figure 3**. PL spectra of polymeric green-LEDs by using (A-C) DDAB- and (A'-C') BDAB-color converters (A,A') by varying the applied voltage. (PL peak position at 521 nm). (B'B) Normalized PL emission stability (PL peak position at 521 nm) of the green-LED devices by applying a constant voltage of 3.0 V at different operational times. The inset of Figure 3B,B' exhibits the characteristic green luminescence of the respective color converter under LED operation. Normalized PL emission stability of (C) polymeric white- and (C') red-LEDs by using anion-exchanged (A-E) color converters by applying a constant voltage of 3.0 V at different operational times. Inset of Figure 3C shows the white luminescence of the A-E-DDAB color converter, measured at 588 nm, while the inset of Figure 3C' displays the red luminescence of the A-E-BDAB color converter measured at 632 nm. The peak at 446 nm is ascribed to the PL emission of the commercial blue LED chip.

For the second type of light emitting applications, LEDs, the AlkylBr-PNCs-$C_xOH$ dispersions were centrifugated, recovering the respective NPs powder from supernatant, and concentrating at 10 mgmL$^{-1}$ in hexane for further use. This concentration was prepared to avoid PNCs aggregation during the layer deposition. Then, the PNCs active layers were integrated in the following configuration: PEDOT:PSS/Poly-TPD/PNCs/POT2T/LiF/Al.[54] In this context, the band alignment is displayed in **Figure S14**A, guaranteeing the carrier mobility into the green-LED devices. Additionally, we prepared diverse batches of LEDs to prevent the influence of the thickness of the active, hole and electron transporting layers. **Figure 4A,B** illustrates the maximum performance of PNCs-based LEDs in the presence of DDAB (L= 10340 cd·m$^{-2}$, J= 828 mA·cm$^{-2}$, and EQE = 23.2%) and BDAB ligands (L= 4363 cd·m$^{-2}$, J= 1324 mA·cm$^{-2}$, and EQE = 20.3%), both types of devices showed a turn-on voltage ($V_{ON}$) of 2.5 V. The corresponding electroluminescence (EL) spectra of the green-LEDs are shown in **Figure S14B,C**. As we have thoroughly exposed in XPS analysis, DDAB favors an efficient surface passivation in the PNCs, producing a PNCs active layer containing a low content of halide defects. In consequence, the carrier injection into the DDAB-LED will be facilitated, improving the radiative recombination by the emergence of a lower density of energy traps. In contrast, the fact that BDAB provides a partial surface coverage, produces that certain NPs exhibit a higher density of non-radiative recombination centers, favoring the carrier trapping (electron accumulation) into the PNCs active layer, limiting the increase of *L* compared with DDAB. The electron trapping induced by the non-radiative channels can facilitate the current leakage, as result of the unbalanced carrier injection towards the perovskite.[55] This can explain the emergence of the roll-off effect at lower currents for the LED device with BDAB compared with DDAB, **see Figure 4B**, indicating a faster current leakage. Surprisingly, by measuring *L* of both AlkylBr-LEDs in function of time at an initial luminance ($L_0$) = 1000 cd·m$^{-2}$, see **Figure 4C**, it is noticeable that a more than one order better operational half lifetime ($t_{50}$) is obtained in the presence of the BDAB, $t_{50}$ = 22 min, than that of DDAB ligand, $t_{50}$ = 1 min. This behavior is similar to the achieved one for down-converting PNCs layers, confirming that the stronger surface binding ability of the $BDA^+$ cation to PNCs delays the decrease of the efficiency in the green-LEDs. Other points contributing to the higher stability can be associated with the presence of benzyl group contained into the BDAB and the lower surface capping coverage, facilitating the carrier transport through the LED along the time.

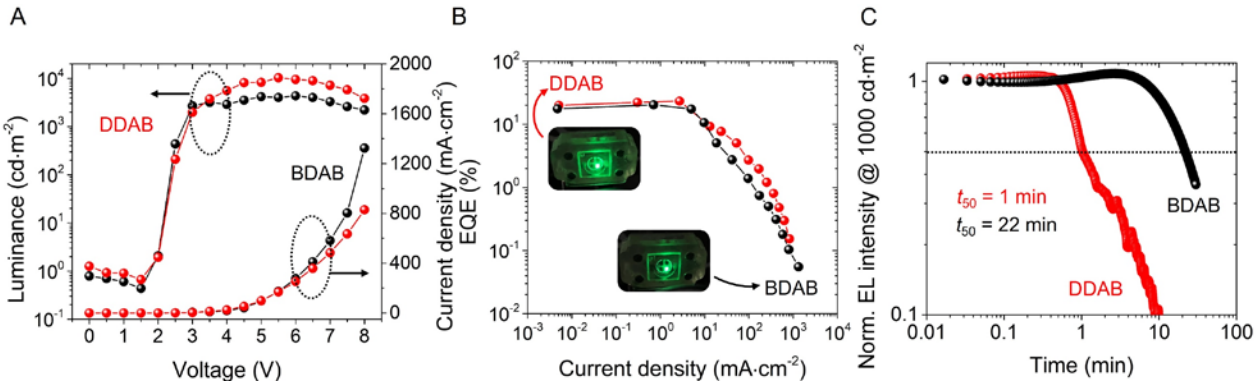


**Figure 4**. (A) J−V−L characteristics and (B) EQE *vs.* J curves of layer-by-layer green-LEDs devices by using DDAB- (red curves) and BDAB-capped (black curves) $CsPbBr_3$ PNCs active layers. Inset of Figure 4B depicts the corresponding devices under operation. (C) Operational stability for the DDAB- and BDAB-green-LEDs by measuring their EL at $L_0$ = 1000 cd·m$^{-2}$.

Lastly, we tried to fabricate efficient electrical driven red-LEDs by passivating $CsPbI_3$ PNCs with both of the AlkylBr capping agents to produce a $CsPbBr_{3-x}I_x$ mixed halide perovskite, but the co-existence of BDAB and MeOH restrains the material redispersion and thereby, avoiding the preparation of the PNCs active layer.[56] NPs aggregation emerges, indicating the removal of a high content of surface ligands in the presence of the alcohol. In this context, only DDAB-capped $CsPbI_3$ could be dispersed to obtain the suitable solution for LED fabrication, using the same device architecture for green-LEDs. As seen in **Figure S15A,B**, we were able to obtain a performance with L= 365 cd·m$^{-2}$, J= 125 mA·cm$^{-2}$ and EQE = 11.8%, with a $V_{ON}$ = 2.5 V, and a EL peak position at 669 nm, see **Figure S15C**. Attending to the fact that iodide-based PNCs are more prone to degrade in contact with polar solvents, a low performance can be reached. However, this is the first report of LEDs composed of alcohol-stable red-emitting $CsPbBr_{3-x}I_x$ PNCs, offering a new insight in the PNCs processing for future optoelectronics. In conclusion, the nature of bulky AlkylBr ligands provides a different surface passivation mechanism in alcohol environments, reaching the stabilization of the PL features in halide PNCs and the fabrication of optical down-converters or architecture-layer LED devices with high performance, being promising for liquid crystal display technologies.

## 3. Conclusions

In this work, we analyze the influence of different AlkylBr ligands such as DDAB, BDAB and TBAB, on the photophysical properties, surface chemistry and stabilization of $CsPbBr_3$ PNCs dispersed in alcohol environments. Depending on the alkylammonium cation nature composing the capping agent, a distinct ligand passivation mechanism was established. We deduce that DDAB provides an efficient compensation of structural defects on the PNCs surface, mainly $Cs^+$ and $Br^-$ sites, removing carrier traps and favoring

radiative recombination. In the case of BDAB, a partial surface coverage is promoted, due to the presence of benzyl groups providing steric hindrance on the material surface. Accordingly, a lower density of this ligand can protect the PNCs against direct interaction with MeOH/BuOH molecules. However, considering that a higher density of free BDAB is available in the dispersion, this ligand can also induce the formation of $R\text{-}O^-$ anions to replace surface $OA^-$ linked to the PNCs. In both bases, we achieve a 100% PLQY and long-term stability around 10 months. Conversely, TBAB offers a poor protection of the PNCs in the polar solvent, presenting a higher degree of steric hindrance through its structure. This feature makes unfavorable the defect passivation, favoring the fast quenching of the PL features in the photomaterial. By using DDAB and BDAB, we prepare efficient green-color converters and LEDs, reaching a slightly higher optical performance for the DDAB-PNCs layers than for BDAB-PNCs. The ligand passivation given by DDAB favors the formation of an active layer with less defects, enhancing radiative recombination and facilitating carrier mobility into the devices. At this point, a maximum EQE of 23.2 and 20.3% was obtained by using DDAB and BDAB, respectively. Nevertheless, in terms of stability, BDAB-PNCs layers present a significantly better capability to resist continuous irradiation and extend the operational performance of the LED device 20-fold longer than DDAB, considering the stronger surface binding of BDAB to the perovskite surface. By extrapolating the surface passivation concept to another kind of PNCs systems, we also obtain efficient stable-alcohol $CsPbBr_{3-x}I_x$ color-converters with typical PL features, and active layers for the fabrication of red-LEDs devices, depicting a EQE ~11.8%. This contribution paves the way for a novel PNCs processing strategy to prepare alcohol-stable multicolor $CsPbX_3$ PNCs with enhanced stability for light emitting applications, as LEDs or LCD technologies.

ASSOCIATED CONTENT

**Supporting Information**. Experimental setup, histograms, SAED patterns, 2D GIWAX data, optical properties, XPS survey and $^1H$ NMR spectra, and theoretical calculations, of the $CsPbBr_3$ PNCs in the presence of the AlkylBr ligands; relative PL intensity and anion-exchange process for color converters, band structure, EL intensity and device performance for $CsPbBr_3$ and $CsPbBr_{3-x}I_x$ PNCs in the presence of DDAB and BDAB ligands, respectively.

**Author contributions**

A.F.G-R., I. O.-R. and J. M. designed the experiments. A.F.G.-R., A.V.-A and O. S. synthesized and characterized the $CsPbX_3$ PNCs. P. U.-V. and C. S. prepared and characterized the alcohol dispersions. F. W., K. R. A., R. C., J. M. and O. S. T. designed and performed the NMR analysis. A.F.G-R., M.E.F. and C. S. fabricated and characterized the $CsPbX_3$ color converters, respectively. A. V.-A. and O.S. fabricated and characterized the LEDs. B. P., C. S., M. P. and J. H performed and analyzed the synchrotron

measurements. C. E.-A. developed the theoretical calculations. M. E. F., S. D. A., S. M. and I. M.-S. contributed to the analysis of material characterization. J.R.-P. contributed to the XPS measurements and analysis. All authors contributed to writing the manuscript and the discussions. P. U.-V. and A. V.-A. have equally contributed to this work.

# P. U.-V. and A.V.-A contributed equally to this work

**Acknowledgements**

This project has been partially supported by the Generalitat Valenciana via Prometeo Grant Q-Solutions (CIPROM/2021/078) and by the Ministerio de Ciencia e Innovación via the project PID2022-140090OB-C21/AEI/10.13039/501100011033/FEDER, EU.". A.F.G.-R. thanks to ANID for the financial support through the FONDECYT Iniciación Project (Grant n°11240161). C.S. is grateful for the FONDECYT Postdoctorado fellowship (Grant n°3220178). F.W. is grateful for the FONDECYT Postdoctorado fellowship 3220023. J.M. thanks to the FONDECYT Iniciación fellowship (Grant n°11230124). O. S. T. is grateful for FONDECYT Regular fellowship 1220241. This work was supported by the Ministry of Science and Innovation of Spain under Projects She-LED (PID2021-122960OA-I00) and Step-Up (TED2021-131600B–C31). S.M. acknowledges financial support from MICINN (Spain) through the program Juan de la Cierva-Incorporación IJC2020-042618-I. O. S. acknowledges funding from the Generalitat Valenciana under a Grisolia pre-doctoral contract reference CIGRIS/2022/122. The authors acknowledge financial support from Generalitat Valenciana (Spain) under Project PRINT-P MFA/2022/020. The authors are very grateful with Vladimir S. Chivrony for his analysis of PL lifetime measurements. We thank to the Unidad de Microscopia Electrónica (UME) of the Universidad Austral de Chile for the TEM and SEM measurements and to Cinthia Quiroga and CEPEDEQ for the usage of NMR facility. We would also like to thank the DELTA for providing synchrotron radiation at beamlines BL2 and BL9.

**References**

[1] A. Dey, J. Ye, A. De, E. Debroye, S. K. Ha, E. Bladt, A. S. Kshirsagar, Z. Wang, J. Yin, Y. Wang, L. N. Quan, F. Yan, M. Gao, X. Li, J. Shamsi, T. Debnath, M. Cao, M. A. Scheel, S. Kumar, J. A. Steele, M. Gerhard, L. Chouhan, K. Xu, X.-g. Wu, Y. Li, Y. Zhang, A. Dutta, C. Han, I. Vincon, A. L. Rogach, A. Nag, A. Samanta, B. A. Korgel, C.-J. Shih, D. R. Gamelin, D. H. Son, H. Zeng, H. Zhong, H. Sun, H. V. Demir, I. G. Scheblykin, I. Mora-Seró, J. K. Stolarczyk, J. Z. Zhang, J. Feldmann, J. Hofkens, J. M. Luther, J. Pérez-Prieto, L. Li, L. Manna, M. I. Bodnarchuk, M. V. Kovalenko, M. B. J. Roeffaers, N. Pradhan, O. F. Mohammed, O. M. Bakr, P. Yang, P. Müller-Buschbaum, P. V. Kamat, Q. Bao, Q. Zhang, R. Krahne, R. E. Galian, S. D. Stranks, S. Bals, V. Biju, W. A. Tisdale, Y. Yan, R. L. Z. Hoye, L. Polavarapu, *ACS Nano* **2021**, 15, 10775.

[2] A. F. Gualdrón-Reyes, S. Masi, I. Mora-Seró, *Trends in Chemistry* **2021**, 3, 499.

[3] E. Scharf, F. Krieg, O. Elimelech, M. Oded, A. Levi, D. N. Dirin, M. V. Kovalenko, U. Banin, *Nano Letters* **2022**, 22, 4340.

[4] J. S. Kim, J.-M. Heo, G.-S. Park, S.-J. Woo, C. Cho, H. J. Yun, D.-H. Kim, J. Park, S.-C. Lee, S.-H. Park, E. Yoon, N. C. Greenham, T.-W. Lee, *Nature* **2022**, 611, 688.
[5] Q. Wan, W. Zheng, C. Zou, F. Carulli, C. Zhang, H. Song, M. Liu, Q. Zhang, L. Y. Lin, L. Kong, L. Li, S. Brovelli, *ACS Energy Letters* **2023**, 8, 927.
[6] H. Aqoma, S.-H. Lee, I. F. Imran, J.-H. Hwang, S.-H. Lee, S.-Y. Jang, *Nature Energy* **2024**, 9, 324.
[7] S. Gao, B. Wang, F. Chen, G. He, T. Zhang, L. Li, J. Li, Y. Zhou, B. Feng, D. Mei, J. Yu, *Angewandte Chemie International Edition* **2024**, 63, 202319996.
[8] L. Ding, C. Shen, Y. Zhao, Y. Chen, L. Yuan, H. Yang, X. Liang, W. Xiang, L. Li, *Molecular Catalysis* **2020**, 483, 110764.
[9] H. Bian, D. Li, S. Wang, J. Yan, S. Liu, *Chemical Science* **2022**, 13, 1335.
[10] N. H. Makani, M. Singh, T. Paul, A. Sahoo, J. Nama, S. Sharma, R. Banerjee, *Journal of Electroanalytical Chemistry* **2022**, 920, 116583.
[11] X. Zhu, Y. Lin, J. San Martin, Y. Sun, D. Zhu, Y. Yan, *Nature Communications* **2019**, 10, 2843.
[12] Y. Lin, J. Guo, J. San Martin, C. Han, R. Martinez, Y. Yan, *Chemistry – A European Journal* **2020**, 26, 13118.
[13] C. Lee, Y. Shin, A. Villanueva-Antolí, S. Das Adhikari, J. Rodriguez-Pereira, J. M. Macak, C. A. Mesa, S. Giménez, S. J. Yoon, A. F. Gualdrón-Reyes, I. Mora-Seró, *Chemistry of Materials* **2021**, 33, 8745.
[14] A. F. Gualdrón-Reyes, J. Rodríguez-Pereira, E. Amado-González, J. Rueda-P, R. Ospina, S. Masi, S. J. Yoon, J. Tirado, F. Jaramillo, S. Agouram, V. Muñoz-Sanjosé, S. Giménez, I. Mora-Seró, *ACS Applied Materials & Interfaces* **2020**, 12, 914.
[15] D. Cardenas-Morcoso, A. F. Gualdrón-Reyes, A. B. Ferreira Vitoreti, M. García-Tecedor, S. J. Yoon, M. Solis de la Fuente, I. Mora-Seró, S. Gimenez, *The Journal of Physical Chemistry Letters* **2019**, 10, 630.
[16] H. Huang, B. Pradhan, J. Hofkens, M. B. J. Roeffaers, J. A. Steele, *ACS Energy Letters* **2020**, 5, 1107.
[17] H. Li, L. Xiong, J. Li, Y. Lu, Z. Shen, D. Song, S. Zhao, Z. Xu, Z. Liang, B. Qiao, *The Journal of Physical Chemistry Letters* **2023**, 14, 5481.
[18] K. H. Fausia, B. Nharangatt, R. N. Vinayakan, A. R. Ramesh, V. Santhi, K. R. Dhandapani, T. P. Manoj, R. Chatanathodi, D. Jose, K. Sandeep, *ACS Omega* **2024**, *9*, 8417.
[19] D. Chen, K. Xu, M. Yang, J. Hu, R. Li, D. Huang, S. Liang, K. He, L. Yuan, S. Wang, C. Zhou, J. Zhang, H. Zhu, *Chemical Engineering Journal* **2023**, 471, 144848.
[20] A. F. Gualdrón-Reyes, C. A. Mesa, S. Giménez, I. Mora-Seró, *Solar RRL* **2022**, 6, 2200012.
[21] Y. He, Y. J. Yoon, Y. W. Harn, G. V. Biesold-McGee, S. Liang, C. H. Lin, V. V. Tsukruk, N. Thadhani, Z. Kang, Z. Lin, *Science Advances* **2019**, 5, eaax4424.
[22] J. Jang, Y. H. Kim, S. Park, D. Yoo, H. Cho, J. Jang, H. B. Jeong, H. Lee, J. M. Yuk, C. B. Park, D. Y. Jeon, Y. H. Kim, B. S. Bae, T. W. Lee, *Advanced Materials* **2020**, 33, 2005255.
[23] L. Zheng, X. Li, X. Lian, R. Xu, X. Liu, T. Xuan, R. Zeng, W.-X. Ni, B. Luo, *Langmuir* **2022**, 38, 15747.
[24] P. Cao, B. Yang, F. Zheng, L. Wang, J. Zou, *Ceramics International* **2020**, 46, 3882.
[25] B. Luo, Y. C. Pu, S. A. Lindley, Y. Yang, L. Lu, Y. Li, X. Li, J. Z. Zhang, *Angewandte Chemie International Edition* **2016**, 55, 8864.
[26] H. Hu, M. Chen, N. Yao, L. Wu, Q. Zhong, B. Song, M. Cao, Q. Zhang, *ACS Applied Materials & Interfaces* **2021**, 13, 4017.
[27] S. Sansoni, F. M. Anoè, M. Meneghetti, *Nanoscale Advances* **2022**, 4, 5009.
[28] A. F. Gualdrón-Reyes, R. Fernández-Climent, S. Masi, C. A. Mesa, C. Echeverría-Arrondo, F. Aiello, F. Balzano, G. Uccello-Barretta, J. Rodríguez-Pereira, S. Giménez, I. Mora-Seró, *Advanced Optical Materials* **2023**, *11*, 2203096.
[29] X. Zhang, X. Bai, H. Wu, X. Zhang, C. Sun, Y. Zhang, W. Zhang, W. Zheng, W. W. Yu, A. L. Rogach, *Angewandte Chemie International Edition* **2018**, 57, 3337.
[30] F. Fang, W. Chen, Y. Li, H. Liu, M. Mei, R. Zhang, J. Hao, M. Mikita, W. Cao, R. Pan, K. Wang, X. W. Sun, *Advanced Functional Materials* **2018**, 28, 1706000.

[31] X. Liu, Z. Luo, W. Yin, A. P. Litvin, A. V. Baranov, J. Zhang, W. Liu, X. Zhang, W. Zheng, *Nanoscale Advances* **2020**, 2, 1973.
[32] P. Papagiorgis, M. Sergides, A. Manoli, M. Athanasiou, C. Bernasconi, F. Galatopoulos, A. Ioakeimidis, C. Nicolaides, E. Leontidis, T. Trypiniotis, S. Choulis, M. I. Bodnarchuk, M. V. Kovalenko, A. Othonos, G. Itskos, *Advanced Optical Materials* **2023**, 12.
[33] C. Collantes, W. Teixeira, V. González Pedro, M.-J. Bañuls, Á. Maquieira, *Applied Materials Today* **2023**, 31, 101775.
[34] T. Chiba, Y. Takahashi, J. Sato, S. Ishikawa, H. Ebe, K. Tamura, S. Ohisa, J. Kido, *ACS Applied Materials & Interfaces* **2020**, 12, 45574.
[35] Y. Miao, Y. Chen, H. Chen, X. Wang, Y. Zhao, *Chemical Science* **2021**, 12, 7231.
[36] S. Y. Lee, S. H. Jang, G. Lee, N.-h. Park, J. Park, D. H. Park, K. H. Cho, J. W. Jung, J. Choi, *Ultrasonics Sonochemistry* **2022**, 89, 106145.
[37] T. C. A. da Silva, C. Fernández-Saiz, R. S. Sánchez, A. F. Gualdrón-Reyes, I. Mora-Seró, B. Julián-López, *Journal of Sol-Gel Science and Technology* **2023**, https://doi.org/10.1007/s10971-023-06171-1.
[38] D. Baranov, G. Caputo, L. Goldoni, Z. Dang, R. Scarfiello, L. De Trizio, A. Portone, F. Fabbri, A. Camposeo, D. Pisignano, L. Manna, *Chemical Science* **2020**, 11, 3986.
[39] A. Dutta, S. K. Dutta, S. Das Adhikari, N. Pradhan, *ACS Energy Letters* **2018**, 3, 329.
[40] J. C. Dahl, X. Wang, X. Huang, E. M. Chan, A. P. Alivisatos, *Journal of the American Chemical Society* **2020**, 142, 11915.
[41] Y. Zhang, W. Zhang, Y. Ye, K. Li, X. Gong, C. Liu, *Solar Energy Materials and Solar Cells* **2022**, 238, 111619.
[42] S. K. Balakrishnan, P. V. Kamat, *Chemistry of Materials* **2017**, 30, 74.
[43] J. Chen, X. Huang, Z. Xu, Y. Chi, *ACS Applied Materials & Interfaces* **2022**, 14, 33703.
[44] H. Kim, J. H. Park, K. Kim, D. Lee, M. H. Song, J. Park, *Advanced Science* **2021**, 9, 210466.
[45] Y.-M. Chen, Y. Zhou, Q. Zhao, J.-Y. Zhang, J.-P. Ma, T.-T. Xuan, S.-Q. Guo, Z.-J. Yong, J. Wang, Y. Kuroiwa, C. Moriyoshi, H.-T. Sun, *ACS Applied Materials & Interfaces* **2018**, 10, 15905.
[46] V. Naresh, S. Singh, H. Soh, J. Lee, N. Lee, *Materials Today Nano* **2023**, 23, 100364.
[47] Y.-H. Chen, J.-Q. Shen, X.-L. Chen, L. Tang, N. Zhang, J.-Y. Zhang, Z.-J. Liu, *Sustainable Energy & Fuels* **2023**, 7, 5499.
[48] H. Wu, Y. Zhang, M. Lu, X. Zhang, C. Sun, T. Zhang, V. L. Colvin, W. W. Yu, *Nanoscale* **2018**, 10, 4173.
[49] F. Zaccaria, B. Zhang, L. Goldoni, M. Imran, J. Zito, B. van Beek, S. Lauciello, L. De Trizio, L. Manna, I. Infante, *ACS Nano* **2022**, 16, 1444.
[50] C. A. Aranda, A. O. Alvarez, V. S. Chivrony, C. Das, M. Rai, M. Saliba, *Joule* **2024**, 8, 241.
[51] Y. Huang, W. Luan, M. Liu, L. Turyanska, *Journal of Materials Chemistry C* **2020**, 8, 2381.
[52] P. Chenna, S. Gandi, S. Pookatt, S. R. Parne, *Materials Today Electronics* **2023**, 5, 100057.
[53] R. An, F. Zhang, X. Zou, Y. Tang, M. Liang, I. Oshchapovskyy, Y. Liu, A. Honarfar, Y. Zhong, C. Li, H. Geng, J. Chen, S. E. Canton, T. Pullerits, K. Zheng, *ACS Applied Materials & Interfaces* **2018**, 10, 39222.
[54] K. M. M. Salim, E. Hassanabadi, S. Masi, A. F. Gualdrón-Reyes, M. Franckevicius, A. Devižis, V. Gulbinas, A. Fakharuddin, I. Mora-Seró, *ACS Applied Electronic Materials* **2020**, 2, 2525.
[55] X. Shen, K. Kang, Z. Yu, W. H. Jeong, H. Choi, S. H. Park, S. D. Stranks, H. J. Snaith, R. H. Friend, B. R. Lee, *Joule* **2023**, 7, 272.
[56] Y. Zhang, L. Chouhan, E. Fron, L. Leoncino, K. Elkhouly, H. Bhatia, W. Qiu, M. B. J. Roeffaers, J. Hofkens, E. Debroye, B. Pradhan, *ACS Photonics* **2023**, 10, 2774.